Available online at www.sciencedirect.com
ScienceDirect
ELSEVIER
Journal of Nuclear Materials 363–365 (2007) 416–420
journal of nuclear materials
www.elsevier.com/locate/jnucmat

Compatibility of the radiating divertor with high performance plasmas in DIII-D

T.W. Petrie [a,*], M.R. Wade [a], N.H. Brooks [a], M.E. Fenstermacher [b], M. Groth [b], A.W. Hyatt [a], R.C. Isler [c], C.J. Lasnier [b], A.W. Leonard [a], M.A. Mahdavi [a], G.D. Porter [b], M.J. Schaffer [a], J.G. Watkins [d], W.P. West [a], DIII–D Team

[a] *General Atomics, P.O. Box 85608, San Diego, CA 92186-5608, USA*
[b] *Lawrence Livermore National Laboratory, Livermore, CA, USA*
[c] *Oak Ridge National Laboratory, Oak Ridge, TN, USA*
[d] *Sandia National Laboratories, Albuquerque, NM, USA*

Abstract

A radiating divertor approach was successfully applied to high performance 'hybrid' plasmas [M.R. Wade et al., in: Proceedings of the 20th IAEA Fusion Energy Conference, Vilamoura, Portugal, 2004]. Our techniques included: (1) injecting argon near the outer divertor target, (2) enhancing the plasma flow into the inner and outer divertors by a combination of particle pumping and deuterium gas puffing upstream of the divertor targets, and (3) isolating the inner divertor from the outer by a structure in the private flux region. Good hybrid conditions were maintained, as the peak heat flux at the *outer* divertor target was reduced by a factor of 2.5; the peak heat flux at the *inner* target decreased by 20%. This difference was caused by a higher concentration of argon at the outer target than at the inner target. Argon accumulation in the main plasma was modest ($n_{Ar}/n_e \leqslant 0.004$ on axis), although the argon profile was more peaked than the electron profile.

PACS: 52.25.Vy; 52.25.Xz; 52.40.Hf; 52.55.Fa; 52.55.Rk

Keywords: Argon; Divertor; Divertor plasma; Impurity screening; DIII-D

---

1. Introduction

Excessive thermal power loading on the divertor structures presents a design problem for future, high-powered tokamaks such as ITER. This problem may be mitigated by 'seeding' the divertor with impurities that radiate a significant fraction of the power upstream of the divertor targets. For this radiating divertor concept to be practical, the confinement and stability of the plasma cannot be compromised by significant leakage of the seeded impurity out of the divertor and into the main plasma. This leakage can be reduced by enhancing the flow of deuterium ions (D^+) into the divertor with a combination of upstream deuterium (D_2) gas puffing and particle pumping at the divertor targets, i.e., 'puff-and-pump' [1–3]. This increase in

---

[*] Corresponding author. Fax: +1 858 455 4156.
E-mail address: petrie@fusion.gat.com (T.W. Petrie).

0022-3115/$ - see front matter © 2007 Elsevier B.V. All rights reserved.
doi:10.1016/j.jnucmat.2007.01.131

the flow raises the frictional force on impurities that inhibits their escape from the divertor. Such an approach may be particularly effective in a closed divertor, where baffling minimizes the direct paths of impurity atoms back into the main chamber.

We report here on the successful application of the puff and pump scenario to plasmas in the 'hybrid' H-mode regime. The hybrid regime [4] has similarities with the conventional edge localized moding (ELMing) H-mode regimes, such as high confinement, e.g., $H_{\mathrm{ITER89P}} \geqslant 2$, where H_{ITER89P} is the energy confinement normalized to the 1989 ITER L-mode scaling [5]. It mainly differs from the conventional H-mode regime, in that sawteeth are absent (or nearly absent). The absence of sawteeth is favorable to high performance plasma operation, since sawteeth can trigger the deleterious $m = 2$, $n = 1$ neoclassical tearing mode (NTM), which can limit the plasma confinement or even disrupt the plasma (In its place, the less deleterious 3/2 NTM is typically present.). The absence of sawteeth can be problematical, because impurities can accumulate at the plasma center in their absence, and lead to reduced plasma performance [6].

The experimental arrangement and methodology are described in Section 2. In Section 3 we present our results and we discuss them in Section 4.

2. Experimental setup

To optimize hybrid plasma operation in a radiating divertor environment, we take advantage of the plasma shaping and particle pumping capabilities of DIII-D, as well as its closed divertor geometry (Fig. 1). A double-null plasma, cross-sectional shape was biased upward (dRsep = +1.0 cm) to exhaust particles into the two (outer and inner) divertor pumps. To increase the ion D^+ flow toward the upper divertor pumps, D_2 was introduced near the bottom of the vessel. Argon (Ar) was injected directly into the private flux region (PFR) of the upper divertor near the outer divertor target. Argon was selected as the seeded impurity because it radiates effectively at the temperatures prevailing in the divertor and pedestal regions of DIII-D hybrid H-mode plasmas and has a relatively short ionization mean free path. Carbon was the dominant intrinsic impurity in DIII-D discharges.

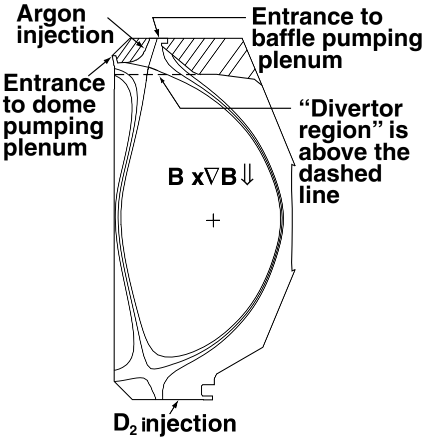

Fig. 1. Particle pumping and gas injection locations are superimposed on the plasma cross-section.

In-vessel pumping of deuterium and Ar was done by cryopumps located in the two upper divertor plenums, indicated by the cross-hatched areas in Fig. 1 [7]. The inner and outer divertor strike points were situated adjacent to the entrances of the dome and baffle plenums. The (upper) divertor is the region above the dashed line in Fig. 1.

Representative parameters were: plasma current $I_p = 1.2$ MA, toroidal field $B_T = 1.7$ T with the $B \times \nabla B$ ion drift directed downward, $q_{95} = 4.3$, power input $P_{IN} = (6.5\text{–}6.9)$ MW, line-averaged density $\bar{n}_e \approx (0.6\text{–}0.7) \times 10^{20}\ \mathrm{m}^{-3}$ (or $\bar{n}_e/n_G \approx$ 0.58–0.63, where n_G is the Greenwald density [8]), and $H_{\mathrm{ITER89P}} = 2.0$. All discharges had Type-1 ELMs [9].

An useful figure of merit to characterize how effectively the injected Ar impurities are kept out of the main plasma is *exhaust enrichment* η_{exh}, defined as $f_{\mathrm{Ar,exh}}/f_{\mathrm{Ar,core}}$. $f_{\mathrm{Ar,core}}$ is the ratio of Ar ion density to electron density in the main plasma and $f_{\mathrm{Ar,exh}}$ is the ratio of the neutral Ar pressure in the outer pump plenum to the atomic-equivalent pressure of D_2 in this plenum. To determine $f_{\mathrm{Ar,core}}$, absolute measurements of the spatial profiles of He-like Ar and fully-stripped carbon densities in the main plasma were made using charge-exchange recombination spectroscopy [10], while the corresponding electron density (n_e) profiles were made by Thomson scattering. To determine $f_{\mathrm{Ar,exh}}$, simultaneous measurements of the Ar and D_2 partial pressures in the exhaust gas were made by a modified Penning gauge located inside the outer plenum [11].

The Ar concentration $f_{\mathrm{Ar,core}}$ was evaluated at radial location $\rho = 0.7$, located ≈10 cm inboard of the outer midplane separatrix. This location was chosen, because analysis with the multiple impurity species transport (MIST) code [12] indicated that helium-like Ar (i.e., Ar^{16+}) was by far the dominant charge state of Ar at $\rho = 0.7$, so that the measured density of Ar^{16+}($n_{\mathrm{Ar}^{16+}}$) would be a good approximation for the *total* Ar density (n_{Ar}) at $\rho = 0.7$.

3. Results

Table 1 summarizes the response of hybrid H-mode plasmas to steady Ar injection rates Γ_{Ar} at a trace level (Case 1) and at two different perturbing levels (Cases 2 and 3). The D_2 gas injection rate Γ_{D_2} was steady. Comparing Case 1 with Case 3 shows that (1) the total radiated power fraction $P_{\mathrm{RAD,TOT}}/P_{\mathrm{IN}}$ increased from 0.45 (Case 1) to 0.63 (Case 3); ≈45% of this increase in $P_{\mathrm{RAD,TOT}}$ between Case 1 and Case 3 came from the radiated power in the main plasma $P_{\mathrm{RAD,MAIN}}$ and ≈40% from the radiated power in the divertor plasma $P_{\mathrm{RAD,DIV}}$, (2) the peak in the conducted heat flux to the outer divertor target $q_{\mathrm{P,OUT}}$, as determined from Langmuir probe data, fell by a factor of ≈2.5, but the peak heat flux at the inner target $q_{\mathrm{P,IN}}$ decreased <20%, (3) the average electron temperature at the *outer* divertor target $T_{\mathrm{e,OUT}}$ decreased from ≈22 eV (Case 1) to ≈10 eV (Case 3), while that at the *inner* target remained $T_{\mathrm{e,IN}} \approx 10$ eV for all three cases. Inner and outer divertor legs were attached during Ar injection in each case, and (4) the Type-1 ELM frequency ν_{ELM} decreased from ≈80 Hz (Case 1) to ≈70 Hz (Case 3).

Fig. 2 shows that $\eta_{\mathrm{exh}}(\rho = 0.7)$ decreased weakly with increasing Γ_{Ar}, and the increase in $n_{\mathrm{Ar}^{16+}}(\rho = 0.7)$ with Γ_{Ar} was slightly faster than linear. The increase in $Z_{\mathrm{eff}}(\rho = 0.7)$ between Case 1 and Case 3 was almost entirely from the additional Ar in the plasma. 'Fuel dilution' due to Ar (i.e., $\approx 16 \times f_{\mathrm{Ar,core}}$) was ≈0.032 at $\rho = 0.7$ in Case 3. As shown in Table 1, the ratio $n_{\mathrm{C}^{6+}}/n_{\mathrm{e}} \approx 0.021$ at $\rho = 0.7$ increased slightly with Γ_{Ar}.

Table 1
Three levels of Ar injection at fixed Γ_{D2}

	Case 1	Case 2	Case 3
Γ_{D_2} (Torr liter/s)	108	108	108
Γ_{Ar} (Torr liter/s)	0.15	1.95	3.8
$\bar{n}_{\mathrm{e}}$ (10^{20} m^{-3})	0.61	0.64	0.67
H_{ITER89P}	2.0	2.0	2.0
P_{IN} (MW)	6.9	6.8	6.6
$P_{\mathrm{RAD,TOT}}/P_{\mathrm{IN}}$	0.45	0.52	0.63
$P_{\mathrm{RAD,MAIN}}/P_{\mathrm{IN}}$	0.17	0.21	0.24
$P_{\mathrm{RAD,DIV}}/P_{\mathrm{IN}}$	0.16	0.18	0.22
$q_{\mathrm{P,IN}}$ (MW/m^2)	1.6	1.5	1.3
$q_{\mathrm{P,OUT}}$ (MW/m^2)	3.0	1.8	1.2
$T_{\mathrm{e,IN}}$ (eV)	10	10	10
$T_{\mathrm{e,OUT}}$ (eV)	22	15	10
ν_{ELM} (Hz)	≈80	≈75	≈70
$n_{\mathrm{C}}/n_{\mathrm{e}}$ ($\rho = 0.7$) (%)	2.1	2.1	2.2
$n_{\mathrm{Ar}}/n_{\mathrm{e}}$ ($\rho = 0.7$) (%)	0.013	0.10	0.20
Z_{eff} ($\rho = 0.7$)	1.65	1.87	2.15
η_{exh}	38	37	33

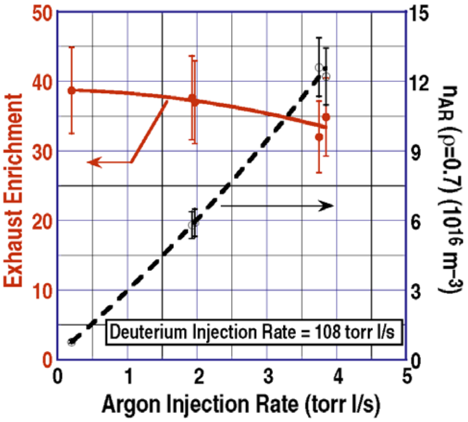

Fig. 2. $\eta_{\mathrm{exh}}(\rho = 0.7)$ and n_{Ar} are shown vs Γ_{Ar}.

The Ar charge state distribution in steady state was evaluated with the MIST code for Case 3. MIST analysis is based on the measured n_{e}, T_{e}, and visible bremsstrahlung profiles, as well as spectrometer data of selected Ar lines [12]. Fig. 3(a) indicates that $n_{\mathrm{Ar}^{16+}}$ was 80–85% of n_{Ar} at location 45 cm, which corresponds to $\rho \approx 0.7$. Near the plasma center, the Ar^{17+} and Ar^{18+} states became significant contributors to n_{Ar}. Ar^{14+} and Ar^{15+} gained in relative importance near the edge. The n_{Ar}-profile, based on MIST analysis, was clearly more peaked than the n_{e}-profile (Fig. 3(b)).

As Γ_{Ar} was raised, most of the increase in the bolometrically-determined radiative emissivity $\varepsilon_{\mathrm{RAD}}$ occurred near the magnetic axis and near the plasma edge (Fig. 4). MIST analysis for Case 3 shows that >80% of the *increase* in the measured $\varepsilon_{\mathrm{RAD}}(\rho = 0)$ came from the line radiation of the Ar^{16+} and Ar^{17+} charge states, while several lower Ar charge states were strong contributors to the increase in $\varepsilon_{\mathrm{RAD}}$ near the edge. The Ar emissivity profile $\varepsilon_{\mathrm{RAD,Ar}}$, as calculated by MIST, was peaked at the center and near the edge of the plasma with a deep trough between (Fig. 3(c)). This is consistent with the changes in the measured $\varepsilon_{\mathrm{RAD}}$ profiles between Case 1 and Case 3 (Fig. 4). MIST analysis indicates that the increase in the radiated power from the main plasma between Case 1 and Case 3

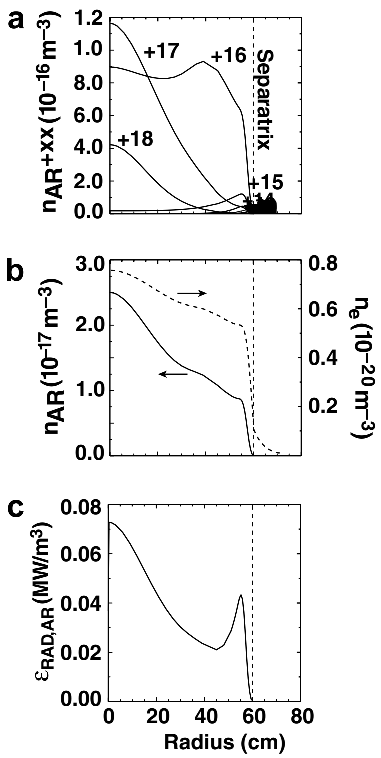

Fig. 3. MIST modeling of Case 3: (a) the density profile of the Ar charge states; (b) the n_{Ar}- and n_e-profiles; (c) the profile of the specific emissivity $\varepsilon_{RAD,Ar}$ due to Ar.

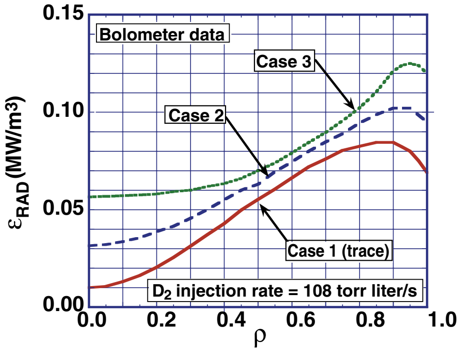

Fig. 4. The bolometrically-measured radiated power densities ε_{RAD} for the 3 cases are plotted vs the normalized radial coordinate ρ.

resulted from the increase in Ar radiation. We estimate the Ar contribution to $P_{RAD,MAIN}$ was ≈30% in Case 3.

Bolometric inversions indicate similarities and differences in the distribution of divertor-radiated power between Case 1 and Case 3. Three areas of strong local emissivity in the divertor were observed: along the inboard divertor leg, along the outboard baffle, and near the outer divertor target. The Case 3 distribution had ≈2.5 times higher emissivity near the *outer* divertor target than Case 1. This local increase in the emissivity was coincident with the reduction in $q_{P,OUT}$. Little change in emissivity along the *inner* divertor separatrix was observed. The reduction in $q_{P,IN}$ was modest (i.e., 15–20%) and could be ascribed largely to the decrease in the conductive/convective power flow out of the main plasma and the increased radiated power in the scrape-off layer plasma (SOL).

Direct measurements of the separate contributions of Ar, carbon, and deuterium to the divertor-radiated power were unavailable. Inferences from available spectroscopic and bolometric data indicate that $P_{RAD,DIV}$ was predominantly from carbon in Case 1. Carbon was the primary radiator in Case 3, where we estimate an *upper* limit of 0.3 for the fraction of Ar radiation to $P_{RAD,DIV}$.

Measurements of Ar emission imply a higher concentration at the entrance to the outer divertor plenum than at the entrance to the inner. The ratio of Ar flux at the outer divertor target $\Phi_{Ar,OUT}$ to that at the inner target $\Phi_{Ar,IN}$ can be estimated by calculating their respective values from $\Phi = I \cdot S(T_e)/X_B(T_e)$, where I is the measured emission rate of the Ar II 434.8 nm line and S/X_B is the ratio of ionization and excitation rates computed from a collisional radiative model [13]. Because the electron temperature and density at *both* divertor targets were comparable in Case 3, i.e., ≈10 eV and $\approx 0.8 \times 10^{20}$ m^{-3}, respectively, then $\Phi_{Ar,OUT}/\Phi_{Ar,IN}$ and $n_{Ar,OUT}/n_{Ar,IN}$ can be roughly estimated as $I_{ArII,OUT}/I_{ArII,IN}$, where $n_{Ar,IN}$ and $n_{Ar,OUT}$ are the Ar densities at the inner and outer targets, respectively. For Case 3, this ratio was ≈6, and the other two cases showed similar strong in/out asymmetry in Ar density.

4. Discussion

Good hybrid conditions were maintained during puff-and-pump in all three cases. Argon puffing directly into the upper outer divertor private flux region, in combination with D$_2$ injection into the upstream SOL and particle pumping at both divertor targets, reduced $q_{P,OUT}$ by about a factor of 2.5 between Case 1 and Case 3. The reduction in $q_{P,IN}$ was ⩽20%. This difference in heat flux reduction resulted from a greater increase in local emissivity near the outer divertor target than near the inner, and resulted from a greater concentration of Ar near the outer target.

Several factors may have contributed to the asymmetric Ar distribution. The Ar source was located in the PFR near the outer divertor target, which, in turn, was adjacent to a major *sink* for the Ar, i.e., the entrance to the outer baffle pumping plenum. For the Ar *neutrals*, direct flight across the PFR from the outer divertor target to the inner was blocked by the presence of the dome. The *ionized* Ar in the PFR near the separatrices would be preferentially dragged toward the outer divertor target, because the $E_R \times B$-induced ionic flow across the PFR is directed from the inner target to the outer. Leakage of Ar out of the closed outer divertor was impeded by the enhanced D^+ flow in the SOL directed into that divertor. Finally, Ar that *does* arrive at the inner target can be exhausted by the dome cryopump. Together, these factors would inhibit a buildup of Ar (and Ar-enhanced radiated power) at the inner target, and explain why a large reduction in $q_{P,IN}$ was not observed.

The accumulation of Ar in the main plasma was almost linear with Γ_{Ar}. One expects n_{Ar} to be roughly proportional to $\Gamma_{Ar} - \Gamma_L(\nu_{ELM})$, where $\Gamma_L(\nu_{ELM})$ is the time-averaged Ar losses from the main plasma during ELMs. If $\Gamma_L(\nu_{ELM})$ were constant as Γ_{Ar} was raised, n_{Ar} would be linear with Γ_{Ar}. However, as more Ar accumulated in the main plasma at higher Γ_{Ar}, $P_{RAD,MAIN}$ increased and ν_{ELM} decreased, so that $\Gamma_L(\nu_{ELM})$ would decrease. The observed reduction in Type-1 ELMing would lead to less effective screening of Ar from the main plasma and a slightly greater than linear response in n_{Ar} to Γ_{Ar}. We also found that the presence of a benign 3/2 NTM did not prevent the n_{Ar}-profile from becoming more peaked than the n_e-profile. Even so, $\varepsilon_{RAD}(\rho)$ was not peaked on axis.

Applying the puff-and-pump approach to hybrid plasmas produced tradeoffs in heat flux reduction, plasma cleanliness, and energy confinement. For the hybrid plasmas discussed, the tradeoffs were favorable, e.g., a sharply reduced $q_{P,OUT}$ while maintaining good energy confinement and low fuel dilution. These favorable results may be helped by the choice of divertor geometry, pumping capability, and the direction of the divertor particle flows.

Acknowledgement

This work was supported by the US Department of Energy under DE-FC02-04ER54698, W-7405-ENG-48, DE-AC05-00OR22725, and DE-AC04-94AL85000.

References

[1] M.J. Schaffer et al., J. Nucl. Mater. 241–243 (1997) 585.
[2] M.R. Wade et al., J. Nucl. Mater. 266–269 (1999) 44.
[3] J.A. Goetz et al., J. Nucl. Mater. 266–269 (1999) 359.
[4] M.R. Wade et al., in: Proceedings of the 20th IAEA Fusion Energy Conference, Vilamoura, Portugal, 2004.
[5] P.N. Yushmanov et al., Nucl. Fusion 30 (1990) 1999.
[6] M.F.F. Nave et al., Nucl. Fusion 43 (2003) 1204.
[7] T.W. Petrie et al., J. Nucl. Mater. 337–339 (2005) 216.
[8] M. Greenwald et al., Nucl. Fusion 28 (1988) 2199.
[9] P. Gohil et al., Phys. Rev. Lett. 61 (1988) 1603.
[10] P. Gohil et al., in: Proceedings of the 14th IEEE/NPSS Symposium on Fusion Engineering, San Diego, 1991, Institute of Electrical and Electronics Engineers, Inc., Piscataway, NJ, 1992.
[11] C.C. Klepper, D.L. Hillis, M.R. Wade, et al., Rev. Sci. Instrum. 68 (1997) 400.
[12] R.A. Hulse, Nucl. Technol. Fusion 3 (1983) 259.
[13] H.P. Summers, Atomic Data and Analysis Structure, JET Joint Undertaking report JET-IR(94)06, 1994.